

Steady-State Diffusion-Weighted Imaging of In Vivo Knee Cartilage

Karla L. Miller,^{1*} Brian A. Hargreaves,¹ Garry E. Gold,² and John M. Pauly¹

Diffusion-weighted imaging (DWI) has strong potential as a diagnostic for early cartilage damage, with clinical impact for diseases such as osteoarthritis. However, in vivo DWI of cartilage has proven difficult with conventional methods due to the short T_2 . This work presents a 3D steady-state DWI sequence that is able to image short- T_2 species with high SNR. When combined with 2D navigator correction of motion-induced phase artifacts, this method enables high resolution in vivo DWI of cartilage. In vivo knee images in healthy subjects are presented with high SNR (SNR = 110) and submillimeter in-plane resolution ($0.5 \times 0.7 \times 3.0 \text{ mm}^3$). A method for fitting the diffusion coefficient is presented which produces fits within 10% of literature values. This method should be applicable to other short- T_2 tissues, such as muscle, which are difficult to image using traditional DWI methods. Magn Reson Med 51:394–398, 2004. © 2004 Wiley-Liss, Inc.

Key words: diffusion MRI; cartilage; navigator; SSFP; knee imaging

The development of tools for diagnosing and monitoring the progression of osteoarthritis (OA) is of considerable clinical interest (1). A number of MRI techniques have been proposed as potential OA diagnostics in recent years. T_2 -mapping can detect collagen loss, but requires long scan times (2). Delayed gadolinium-enhanced MRI of cartilage (dGEMRIC) is sensitive to early changes in proteoglycan content, but is time-consuming and requires a contrast injection (3). Sodium imaging is also useful for imaging proteoglycan depletion, but has low SNR and requires special hardware due to the shifted resonance frequency of sodium (4). A promising alternative to these methods is diffusion-weighted imaging (DWI) (5,6), which reflects tissue structure and may detect early cartilage matrix damage (7,8).

While a number of in vitro studies have been performed (5–10), in vivo DWI of cartilage has proven difficult for two reasons. First, the short T_2 of cartilage (20–40 ms (6)) causes low SNR in standard DWI techniques such as spin echo (SE-DWI), which require long echo times. While this issue can be addressed with extensive averaging in vitro, poor SNR is a significant obstacle for in vivo DWI of cartilage (11). Second, the sensitivity of DWI to even small subject motion makes it difficult to achieve the high resolution needed for the assessment of cartilage. To achieve

the necessary resolution, multishot readouts with navigator motion correction are required (12,13).

This work presents a method for DWI of cartilage that is based on steady-state DWI (SS-DWI) (14). SS-DWI achieves strong diffusion weighting with high SNR for short- T_2 species. Navigated correction of motion artifacts has recently been developed for 2D SS-DWI, enabling high-SNR, high-resolution diffusion images of the brain (15). This work extends the latter technique to 3D, with specific application to knee cartilage. In vivo results are presented, including quantitative measurements of the diffusion coefficient, which has previously proven difficult with SS-DWI (16,17). This sequence enables high-resolution, high-SNR, 3D DWI of in vivo knee cartilage in reasonable imaging times. This method should also be applicable to other short- T_2 tissues, such as muscle, which are difficult to image using traditional DWI methods.

THEORY

This work describes the 3D navigated steady-state DWI sequence diagrammed in Fig. 1. This sequence consists of a slab-selective RF excitation followed by a large, unbalanced diffusion gradient (which can be applied along any direction, but is shown on the z-axis in Fig. 1). This gradient is followed by two readouts, a low-resolution 2D navigator and a high-resolution 3D multishot readout (respectively, a spiral and 3DFT in Fig. 1). The components of this sequence and its application to cartilage imaging are discussed below.

Steady-State DWI

Diffusion weighting is usually added to a pulse sequence with a pair of large gradients with the same area but opposite polarity (referred to as a “bipolar” gradient set). Diffusive motion between the lobes of the bipolar pulse result in phase dispersion, and therefore signal attenuation. SS-DWI is able to obtain similar diffusion weighting with a single, unbalanced gradient (Fig. 1) (14) by creating a steady state in which an effective bipolar set is formed from this single gradient over multiple T_{RS} .

It is helpful to consider the steady-state signal as a summation of echoes, where each echo is described by the orientation of the magnetization (transverse or longitudinal) during the preceding periods. Figure 2a shows an example echo. In this echo, the magnetization excited during the first transverse period is dephased by the diffusion gradient, tipped longitudinal by the next RF pulse, and reenters the transverse plane $4 T_{RS}$ later. The magnetization only forms an echo in this final repetition period, when the diffusion gradient rephases the signal (see Fig. 2b). If spins have diffused during the intervening longitudinal periods, the magnetization is incompletely refo-

¹Department of Electrical Engineering, Stanford University, Stanford, California.

²Department of Radiology, Stanford University, Stanford, California.

*Correspondence to: Karla L. Miller, Packard Electrical Engineering Building, Room 210, Stanford University, Stanford, CA 94305-9510. E-mail: bison@stanford.edu

Received 22 July 2003; revised 29 September 2003; accepted 29 September 2003.

DOI 10.1002/mrm.10696

Published online in Wiley InterScience (www.interscience.wiley.com).

© 2004 Wiley-Liss, Inc.

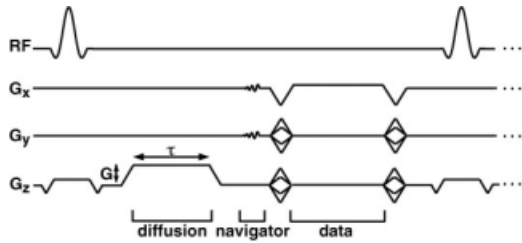


FIG. 1. Navigated 3D SS-DWI pulse sequence with a 3DFT acquisition and a 2D spiral navigator. As the sequence rapidly repeats, the magnetization achieves a diffusion-weighted steady state.

caused, resulting in diffusion contrast. The total signal is a summation of echoes similar to that depicted in Fig. 2a, each with a different number of longitudinal periods. The amount of attenuation a given echo experiences depends on the length of time spins are allowed to diffuse, which is proportional to the number of longitudinal periods. Echoes with a large number of longitudinal periods experience heavy diffusion weighting.

SS-DWI enables the imaging of short- T_2 species, provided the T_1 is not also short. As described above, most of the diffusion weighting in SS-DWI results from the inclusion of echoes with a large number of longitudinal periods. During these longitudinal periods, the signal is decaying according to T_1 rather than T_2 (see Fig. 2c). This mechanism enables strong diffusion weighting with minimal T_2 decay, which is ideal for cartilage.

Diffusion Coefficient Calculations

Since the SS-DWI signal is a weighted summation of many diffusion-weighted echoes, there is a fairly complicated signal dependence on T_1 , T_2 , D , and flip angle (α). While the full signal expression includes all possible echoes with

an even number of transverse periods, the signal is dominated by echoes that experience only two transverse periods (16) (i.e., spin and stimulated echoes). By considering only coherence pathways with two transverse periods, the signal attenuation A_M can be approximated as (16):

$$A_M = \frac{M(G\tau)}{M(0)} = \frac{A_D(1 + A_DE_1)(1 - E_1\cos(\alpha))}{(1 + E_1)(1 - A_DE_1\cos\alpha)} \quad [1]$$

where $A_D = \exp(-(\gamma G\tau)^2 T_R D)$ is the diffusion attenuation factor for a diffusion gradient of strength G and duration τ , and $E_1 = \exp(-T_R/T_1)$. Equation 1 is independent of T_2 since all of the echoes have the same T_2 weighting. This approximation is accurate provided $T_R \geq T_2$ and the flip angle is small. As illustrated in fig. 2 of Ref. 16, the constraint on the flip angle is lessened as the T_R becomes long, albeit with an accompanying loss of SNR.

Equation 1 has a different form from the attenuation of standard DWI methods, for which $A_M = \exp(-bD)$. For convenience of description, we will refer to the diffusion weighting of our sequence with the b -value which would give equivalent attenuation in cartilage ($D = 0.00145 \text{ s/mm}^2$ (6,9)). This allows direct comparison of the diffusion weighting of cartilage in our sequence with standard DWI methods.

Given T_1 , Eq. 1 involves a single unknown, D , which can be fit using standard nonlinear optimization methods. This procedure should be both simpler and less error-prone than previous methods, which have attempted to fit the full expression for the SS-DWI signal using either assumed T_1 and T_2 (16) or phantom calibrations (17). In this study, we assume $T_1 = 800 \text{ ms}$ (9,18) and fit D to Eq. 1 from several measurements with varying diffusion gradient area. As discussed below, simulations indicate that large

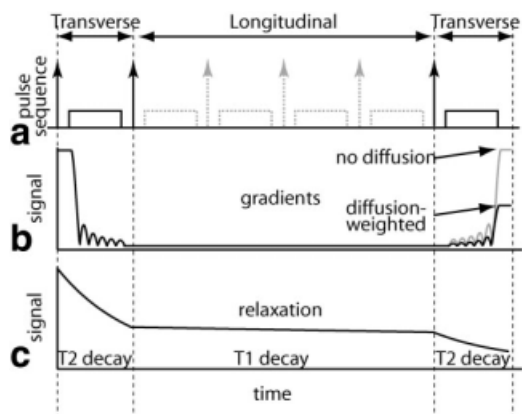


FIG. 2. Relaxation and diffusion gradient effects on an example echo pathway in SS-DWI. **a:** The example echo pathway consists of two transverse periods separated by 4 longitudinal periods. **b:** The diffusion gradient dephases the signal in the first transverse period and rephases the signal to form an echo in the second transverse period. Diffusive motion during the longitudinal periods causes signal attenuation. **c:** The echo decays according to T_1 during the longitudinal periods, allowing long diffusion times without significant signal loss due to T_2 decay.

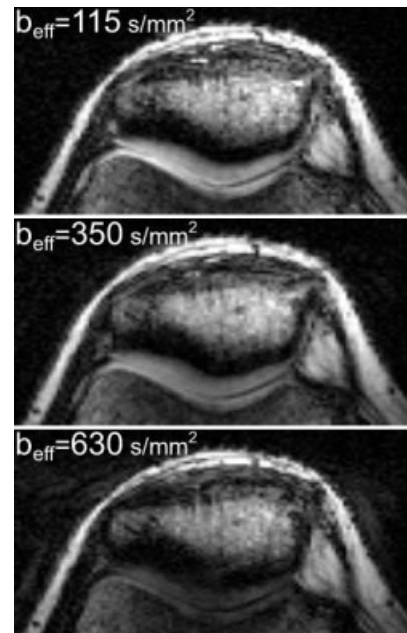


FIG. 3. 3D diffusion-weighted knee images acquired using steady-state DWI with three levels of diffusion weighting. The cartilage signal is attenuated with increasing b .

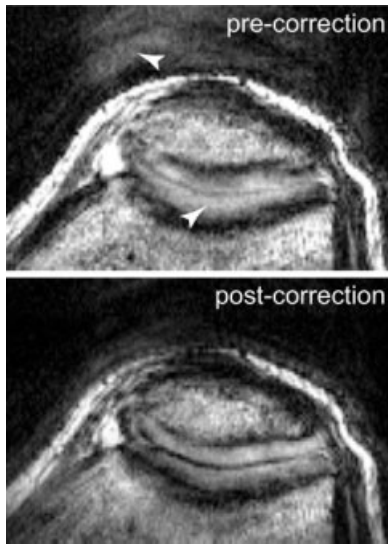


FIG. 4. 3D diffusion-weighted knee images before and after navigator correction. Arrows indicate motion artifacts removed by the correction. The navigator correction removes ghosting and blurring artifacts from the cartilage. These images are windowed harshly to accentuate artifacts.

errors in the T_1 used in the fit introduce a fairly small bias ($\leq 10\%$) to the fitted value of D .

Navigator Correction

Bulk motion in DWI results in phase offsets and causes image artifacts in multishot acquisitions when this phase varies from one readout to another (13). These motion-induced errors can be removed based on a low-resolution, full-FOV phase reference known as a navigator (19). In each excitation, the same navigator is acquired along with the current high-resolution data frame. The navigator is used to correct phase disturbances in the high-resolution data before the individual readouts are combined to make an image. The correction used here is an approximation to the least-squares optimal reconstruction of phase-corrupted DWI data (15).

Removal of all possible phase errors in a 3D dataset would require acquisition of a 3D navigator every T_R . However, motion in the knee is likely to be restricted. The primary motion during scanning is likely to be in the axial

plane, where the knee might rotate or shift. The knee might also shift in the superior–inferior (S/I) direction, but more complex motions in this direction are less likely. Depending on the direction of diffusion encoding, a shift in the S/I direction may cause a constant phase offset, but no higher-order terms (12), indicating that a 2D axial navigator (i.e., at $k_z = 0$) should be sufficient to correct motion-induced phase errors.

MATERIALS AND METHODS

In vivo images of the patellar–femoral joint were acquired in three healthy subjects on a 1.5 T Signa LX scanner (40 mT/m maximum gradient amplitude, 150 T/m/s maximum gradient slew rate) using a 7.5 cm surface coil centered on the patella. Axial images were gathered through the articular cartilage covering a $14 \times 14 \times 4.8$ cm³ FOV in a $256 \times 192 \times 16$ matrix for $0.5 \times 0.7 \times 3.0$ mm² voxel resolution. Spiral navigators were acquired in the $k_z = 0$ plane over a 14×14 cm² FOV in a 4×4 matrix. The SS-DWI sequence utilized $T_R = 30$ ms and $\alpha = 25^\circ$ to satisfy the constraints on Eq. 1. Diffusion gradients of strength $G = 7.8, 15, 27.5,$ and 40 mT/m were applied for $\tau = 5.5$ ms, causing signal attenuation in cartilage equivalent to $b = 30, 115, 350, 630$ s/mm². The subject was stabilized using a knee-high plastic brace loosely mounted on the patient bed. Three averages were acquired for a total scan time for each b -value of 4:40. The diffusion-weighted data was fit on a voxel-by-voxel basis to Eq. 1 using the nonlinear, bounded Golden Section search algorithm (20) provided in Matlab (MathWorks, Natick, MA). The fit used an RMS-error (l_2 -norm) cost function and bounds $0.0 \leq D \leq 0.01$ mm²/s.

RESULTS

Figure 3 shows 3D SS-DWI knee images with varying levels of diffusion weighting obtained on a healthy volunteer. These images have been navigator-corrected to remove motion artifacts. The cartilage has high signal at low levels of diffusion weighting (SNR ≈ 110 in the $b = 30$ s/mm² image), and is attenuated at increasing b -values due to the relatively high diffusion coefficient of cartilage. Navigator correction was crucial in generating usable images, particularly at higher levels of diffusion weighting. Figure 4 shows a typical $b = 630$ s/mm² image before and

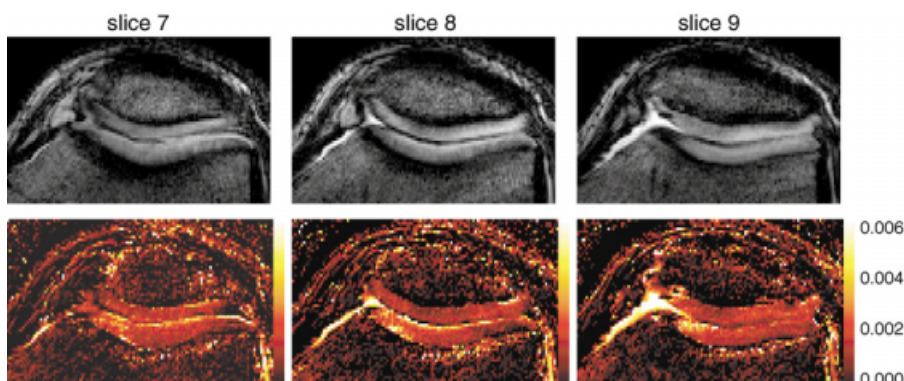


FIG. 5. Diffusion maps for three representative slices in the 3D SS-DWI acquisition (bottom row) along with the $b = 115$ s/mm² images for anatomical references (top row). The values fit for the diffusion coefficient (D) are in the range of literature values (0.00145 mm²/s).

after navigator correction. The navigator correction removes the ghosting and blurring artifacts found in the uncorrected image.

Figure 5 shows diffusion coefficient (D) fits for three contiguous slices from a 3D SS-DWI dataset. The D -maps have high SNR in cartilage, indicating a well-conditioned fit to the data. The average diffusion coefficient over an ROI of pure cartilage (433 voxels identified from the $b = 115$ s/mm² anatomical image) is 0.0016 mm²/s, slightly higher than in vitro literature values of about 0.00145 mm²/s (6,9). This slight overestimate may be due to a bias in the fitting procedure itself, or may simply reflect the existence of synovial fluid in the ROI.

Previous work has reported characteristic spatial heterogeneity in cartilage, with low D and T_2 at the bone-cartilage interface, which increase across the cartilage to peak at the articular surface (2,6). Figure 6 shows the fitted diffusion coefficient (solid lines) and the T_2 -weighted signal from the $b = 115$ s/mm² images (dashed lines) across the cartilage (both femoral and patellar). These results are in good qualitative agreement with previous findings (2,6).

DISCUSSION

Quantification of D with SS-DWI requires care due to the fairly complicated signal dependence on tissue parameters and flip angle (16). To evaluate the sensitivity of our fitting procedure to errors in the flip angle and T_1 , fits were made to simulated data generated from the full expression for the SS-DWI signal (16). Simulations used the imaging parameters from our experiments ($T_R = 30$ ms, $G = 7.8, 15, 27.5, 40$ mT/m, $\tau = 5.5$ ms, $\alpha = 25^\circ$), and the approximate tissue parameters for cartilage ($T_2 = 30$ ms, $T_1 = 800$ ms, $D = 0.0015$ mm²/s). In each fit, either the flip angle or the T_1 used in the fit was varied to simulate the effect of an incorrect estimate of the given parameter. Each fit was repeated 200 times with varying Gaussian noise that matched our experimental SNR ≈ 110 .

The results of these simulations are shown in Fig. 7. The fitting procedure is sensitive to errors in the flip angle (Fig. 7a), reflecting the strong dependence of the diffusion weighting on flip angle. The use of a 3D acquisition essentially removes any slice profile effects that may complicate

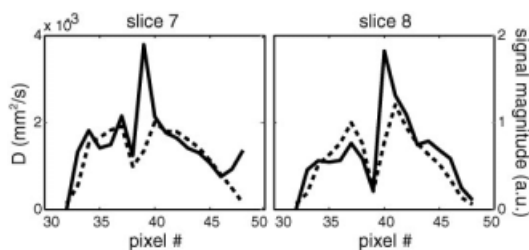


FIG. 6. Average of five adjacent voxel columns through the patellar and femoral cartilage from the images in Fig. 5. Shown are the fitted diffusion coefficient D (solid lines, in mm²/s) and the T_2 -weighted signal from the $b = 115$ s/mm² images (dashed lines, in arbitrary units). The outer pixels correspond to the bone-cartilage interface and the dips in the center occur at the cartilage surface. Both T_2 and D are low at the bone interface and high at the cartilage surface, as previously reported in vitro.

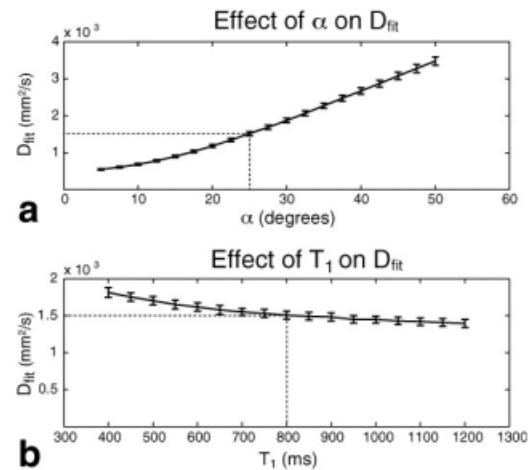


FIG. 7. Sensitivity of the diffusion coefficient fit (D_{fit}) to the flip angle and T_1 used in the fit. Data was simulated as described in the text. The dashed lines in the plots above represent the “actual” values used to generate the simulated data. The diffusion coefficient was fit to the simulated data for a range of (incorrect) values for α and T_1 to evaluate the sensitivity of the fit to errors in these parameters.

the fitting procedure (16). However, quantification of D still requires an accurate flip angle. Careful calibration of the excitation pulse produced the data presented above, which is within 10% literature values. The fitting procedure is largely unaffected by the value of T_1 used in the fit (see Fig. 7b). Although the choice of T_1 introduces a bias to the fit (where underestimating T_1 causes an overestimate of D), this bias is relatively small.

CONCLUSIONS

We have presented a method for diffusion imaging of cartilage based on steady-state DWI (SS-DWI). This method obtains high SNR in vivo images of cartilage with strong diffusion weighting despite the short T_2 of cartilage. Navigator correction of motion artifacts is crucial due to the strong sensitivity of the method to even minor subject motion. We have presented high-SNR 3D in vivo DWI of cartilage with submillimeter in-plane resolution and reasonable scan times. Fitted values of the diffusion coefficient were within 10% of literature values. Quantification with this method requires careful calibration of the flip angle due to the strong sensitivity of SS-DWI to flip angle. This technique should allow for diffusion-weighted imaging of the knee in the clinical setting, and may be useful in other tissues with short- T_2 .

REFERENCES

1. Felson DT, Lawrence RC, Dieppe PA, Hirsch R, Helmick CG, Jordan JM, Kington RS, Lane NE, Nevitt MC, Zhang Y, Sowers M, McAlindon T, Spector TD, Poole AR, Yanovski SZ, Ateshian G, Sharma L, Buckwalter JA, Brandt KD, Fries JF. Osteoarthritis: new insights. 1. The disease and its risk factors. *Ann Intern Med* 2000;133:635–646.
2. Mosher TJ, Dardzinski BJ, Smith MB. Human articular cartilage: influence of aging and early symptomatic degeneration on the spatial variation of T2-preliminary findings at 3 T. *Radiology* 2000;214:259–266.
3. Bashir A, Gray ML, Burstein D. Gd-DTPA²⁻ as a measure of cartilage degradation. *Magn Reson Med* 1996;36:665–673.

4. Reddy R, Insko EK, Noyszewski EA, Dandora R, Kneeland JB, Leigh JS. Sodium MRI of human articular cartilage in vivo. *Magn Reson Med* 1998;39:697–701.
5. Burstein D, Gray ML, Hartman AL, Gipe G, Foy BD. Diffusion of small solutes in cartilage as measured by nuclear resonance (NMR) spectroscopy and imaging. *J Orthop Res* 1993;11:465.
6. Xia Y, Farquhar T, Burtonwurster N, Ray E, Jelinski LW. Diffusion and relaxation mapping of cartilage-bone plugs and excised disks using microscopic magnetic-resonance-imaging. *Magn Reson Med* 1994;31:273–282.
7. Frank LR, Wong EC, Luh WM, Ahn JM, Resnick D. Articular cartilage in the knee: mapping of the physiologic parameters at MR imaging with a local gradient coil—preliminary results. *Radiology* 1999;210:241–246.
8. Mlynarik V, Sulzbacher I, Bittsanky M, Fuiko R, Trattnig S. Investigation of apparent diffusion constant as an indicator of early degenerative disease in articular cartilage. *J Magn Reson Imag* 2003;17:440–444.
9. Henkelman RM, Stanisz GJ, Kim JK, Bronskill MJ. Anisotropy of NMR properties of tissues. *Magn Reson Med* 1994;32:592–601.
10. Knauss R, Schiller J, Fleischer G, Karger J, Arnold K. Self-diffusion of water in cartilage and cartilage components as studied by pulsed field gradient NMR. *Magn Reson Med* 1999;41:285–292.
11. Gold GE, Butts K, Fechner KP, Bergman G, Beaulieu CF, Lang PK, Macovski A. In vivo diffusion-weighted imaging of cartilage. In: *Proc 6th Annual Meeting ISMRM, Sydney, 1998*. p 1066.
12. Ordidge RJ, Helpert JA, Qing ZX, Knight RA, Nagesh V. Correction of motion artifacts in diffusion-weighted MR images using navigator echoes. *Magn Reson Imag* 1994;12:455–460.
13. Anderson AW, Gore JC. Analysis and correction of motion artifacts in diffusion weighted imaging. *Magn Reson Med* 1994;32:379–387.
14. Bihan DL. Intravoxel incoherent motion imaging using steady-state free precession. *Magn Reson Med* 1988;7:346–351.
15. Miller KL, Pauly JM. Nonlinear phase correction for navigated diffusion imaging. *Magn Reson Med* 2003; 50:343–353.
16. Buxton RB. The diffusion sensitivity of fast steady-state free precession imaging. *Magn Reson Med* 1993;29:235–243.
17. Quest RA, McRobbie DW. Investigation of the visual pathways using diffusion-weighted PSIF. In: *Proc 9th Annual Meeting ISMRM, Glasgow, 2001*. p 1548.
18. Diewell SH, Ceckler TL, Ong K, Wen H, Jaffer FA, Chesnick SA, Balaban RS. Musculoskeletal MR imaging at 4 T and at 1.5 T: comparison of relaxation times and image contrast. *Radiology* 1995;196:551–555.
19. Butts K, Pauly J, Crespigny A, Moseley M. Isotropic diffusion-weighted and spiral-navigated interleaved EPI for routine imaging of acute stroke. *Magn Reson Med* 1997;38:741–749.
20. Press WH, Teukolsky SA, Vetterling WT, Flannery BP. *Numerical recipes in C*, 2nd ed. New York: Cambridge University Press; 1994.